文章编号：1001-9014(2023)03-0306-05

DOI:10.11972/j.issn.1001-9014.2023.03.004

Liquid Phase Epitaxy (LPE) growth of the room-temperature InAs-based mid-infrared photodetector

CHEN Ze-Zhong[1], DUAN Yong-Fei[1], LIN Hong-Yu[3], ZHANG Zhen-Yu[1], XIE Hao[2], SUN Yan[2], HU Shu-Hong[2*], DAI Ning[2,4*]

(1. School of Materials and Chemistry, University of Shanghai for Science and Technology, Shanghai 200093, China;
2. Shanghai Institute of Technical Physics of the Chinese Academy of Sciences, Shanghai 200083, China;
3. Zhejiang Lab, Hangzhou 311100, China;
4. Hangzhou Institute for Advanced Study, University of Chinese Academy of Sciences, Hangzhou 310024, China)

Abstract: The material quality is very important to obtain the high performance infrared detector. It is presented that the key issue of the material quality is to control the lattice mismatch between the layers of the device architecture. The effects of the lattice mismatch on the material quality and the dark current characteristics were reported. In the InAs/InAsSbP system grown by LPE technology, there is an appropriate value for the lattice mismatch between InAsSbP and InAs. If the lattice mismatch deviates from this value, no matter whether it is smaller or larger, the material quality will deteriorate. Then it was stated how to adjust growth parameters to obtain the appropriate lattice mismatch. The infrared detector made from the device architecture with the appropriate lattice mismatch was fabricated, and the room-temperature peak detectivity of this detector is 6.8×10^9 cm Hz$^{1/2}$W^{-1} at zero bias, which is comparable with that of international commercial InAs photodetectors.

Key words: semiconducting quaternary alloys, infrared detector, liquid phase epitaxy, lattice mismatch

InAs基室温中波红外探测器的液相外延生长

陈泽中[1], 段永飞[1], 林虹宇[3], 张振宇[1], 谢 浩[2], 孙 艳[2], 胡淑红[2*], 戴 宁[2,4*]

(1. 上海理工大学 材料与化学学院,上海 200093;
2. 中国科学院上海技术物理研究所,上海 200083;
3. 之江实验室,浙江 杭州 311100;
4. 中国科学院大学杭州高等研究院,浙江 杭州 310024)

摘要:材料质量好坏对于获得高性能红外探测器至关重要。提出决定材料质量的关键点在于精准控制材料结构中层与层之间的晶格失配度,报道了晶格失配对材料质量和器件暗电流性能的影响。实验结论表明在液相外延技术生长的InAs/InAsSbP材料体系中,InAs和InAsSbP间的晶格失配不是越小越好,而是有一个最佳值。如果晶格失配偏离这个值,不管是偏大还是偏小,材料的质量都会恶化。阐述了如何调整生长参数以获得合适的晶格失配度。制备了具有适宜晶格失配度的红外探测器件,该探测器零偏压下的室温峰值探测率为6.8×10^9 cm Hz$^{1/2}$W^{-1},与国际商用InAs探测器的指标相当。

关 键 词:半导体四元合金;红外探测器;液相外延;晶格失配

中图分类号:O78　　**文献标识码**:A

Received date: 2022-10-13, **revised date**: 2023-02-13　　**收稿日期**:2022-10-13,**修回日期**:2023-02-13

Foundation items: Supported by the National Natural Science Foundation of China (11933006), the Frontier Science Research Project (Key Programs) of the Chinese Academy of Sciences (QYZDJ-SSW-SLH018), the National Natural Science Foundation of China (U2141240)

Biography: CHEN Ze-Zhong (1971-), male, Jiangxi China, Ph. D. Research area involves metal plastic forming CAE and CAD/CAM, E-mail: zzhchen@usst.edu.cn

* **Corresponding authors**: E-mail: hush@mail.sitp.ac.cn, ndai@mail.sitp.ac.cn

Introduction

Infrared detectors that operate in the middle-wavelength infrared (MWIR) range are essential for many applications, such as satellite communications, target tracking, and object identification[1-3]. Mercury Cadmium Telluride (HgCdTe) detectors are dominant in infrared photoelectric detection[4-5], however, they are limited by low operating temperatures. InAs-based MWIR detectors are now preferred for room-temperature applications due to the introduction of a new type of device structure [6-8]. There are two types of InAs-based infrared detectors reported in recent years, one uses AlAsSb-based alloy as barrier grown by Molecular Beam Epitaxy (MBE) technology[9-15], which needs driving voltage, and the other uses InAsSbP alloy as barrier grown by LPE technology[16-17], which can work at zero bias voltage.

In Ref. [16], we presented a high-performance room-temperature InAs-based infrared photodetector, the room-temperature peak detectivity of the photodetector is as high as 1.6×10^{10} cm $Hz^{1/2}W^{-1}$ at zero bias. We all know that device performance is strongly dependent on the quality of device materials, however, there are few reports on the growth details of InAs-based detectors, whether LPE growth or MBE growth[18]. In this work, firstly we studied the surface defects of InAsSbP epilayer when the lattice mismatch between InAsSbP and InAs deviates from the appropriate value. Secondly, we state how to adjust growth parameters to obtain the appropriate lattice mismatch. Thirdly, we gave the *I-V* curves of the device to verify the dark current characteristic of the device architecture with different lattice match. Lastly, we fabricated the infrared detector made from the device architecture with appropriate lattice mismatch and measured its room-temperature detectivity.

1 Experiments

The samples were grown on (100)-oriented InAs substrate by LPE technology, using a conventional horizontal sliding graphite boat. The precursors for the growth melts were undoped polycrystalline InAs, InP, and 7 N pure Indium (In) and Antimony (Sb). InAs substrates were rinsed successively with acetone, isopropanol, and deionized water. They were then etched using a mixture solution (H_2O_2: HNO_3 = 5: 3) to remove the native oxide layer on their surface. Prior to the epitaxial growth, the source materials were baked at 650 ℃ for 2.5 hours under a purified hydrogen gas flow (hydrogen gas purifier: Simpure 9NP050-H) to homogenize and remove the volatile impurities. Growth was initiated at 550 ℃ using the supercooling technique.

The structural properties of the epilayers were investigated by high-resolution X-ray diffraction (HRXRD) measurements (D8/Discover 2 000, Bruker, Germany). Only Cu $K_{\alpha1}$ line (λ=1.540 6 Å) was provided through the Ge (220) monochromator. The cross-section micrographs of device samples were observed by scanning electronic microscopy (SEM) (Sirion 200D1615, FEI, USA) measurements. Before the SEM observation, the samples were corroded using the corrosive A-B solution (A: 40 cm^3 H_2O + 0.3g $AgNO_3$+40 cm^3 HF and B: 40g CrO_3+ 40 cm^3 H_2O) for 3 seconds to display clear interfaces. The resulting structure was processed into 200 μm-diameter mesa-etched photodiodes using conventional photolithography and processing techniques. Ohmic contacts were formed by the thermal evaporation of Cr/Au. No attempts were made to passivate the surfaces. The spectral response was measured using a Nicolet Is50 FTIR spectrometer. The light emitted by a blackbody source passed through the interferometer and was collected by the device. The detectivity D^* was measured using a blackbody temperature of 900 K, a testing bandwidth of 100 Hz, and a modulation frequency of 1000 Hz.

2 Results and discussions

2.1 LPE growth of InAsSbP epilayer on InAs substrate

A serial of samples with the different lattice mismatches of 0.4-0.07% were grown by LPE technology. Figure 1(a) shows the HRXRD patterns of samples S1-S6 and Fig. 1(b) shows rocking curves of InAsSbP epilayer of samples S1-S6. We note that the full width at half maximum (FWHM) value of InAsSbP epilayer for sample S3 with the lattice mismatch of 0.22% is comparable to that of InAs substrate, indicating the high quality of the crystalline lattice for InAsSbP epilayer of this sample. For samples with the lattice mismatches deviating from the value of 0.22%, whatever the lattice mismatch is smaller or larger than 0.22%, the FWHM is significantly widened, which means that the crystalline quality of InAsSbP epilayer becomes poor. It is easy to understand that when the lattice mismatch increases, the FWHM widens and the quality of the crystalline lattice becomes poor, but it is surprising that the decrease of the lattice mismatch has also led to the increase of the FWHM. Figure 2 shows the surface morphology of samples S1-S6. It can be seen that the surface morphology of InAsSbP epilayer is strongly dependent on the lattice mismatch between InAsSbP and InAs. When the lattice mismatch increases along the positive mismatch direction, crosshatch pattern begins to appear, which develops from faint to clear with the increase of lattice mismatch, as shown in sample S1 and S2 in Fig. 2. Crosshatch pattern is a typical morphology of epilayer grown by LPE technology, which is closely related to the presence of interfacial dislocation[19]. It is normally considered that the smaller the lattice mismatch between hetero-epitaxial layers, the easier it is to obtain the epilayer with low defect density. In InAsSbP/InAs system, however, when the lattice mismatch continues to decrease, some bulge-like defects appeared on the surface, as shown in sample S5 in Fig. 2. As the lattice mismatch is close to zero, the bulge-like defects density increases fast and the morphology became poor as shown in sample S6 in Fig. 2. However the formation mechanism of the bulge-like defects in InAsSbP/InAs system is not very clear. The InAsSbP epilayer with shiny uniform surface only could be obtained in the condition of slight positive lattice mismatch, the value of

which is about 0.2% in our work.

2.2 LPE growth of the device material

We have designed the three device samples D1-D3 with different lattice mismatch of 0.09%, 0.21% and 0.40%. We intend to study how the detector performance will be when the lattice mismatch deviates from the appropriate value of about 0.2%. Figure 3 shows the structure schematic of the device samples. The growth started with a 1.2-1.5 μm InAsSbP barrier layer, and then 3-4 μm undoped InAs absorption layer was grown, a 700-800 nm highly doped n-type InAsSbP window layer was grown at the last step. The key to the design of this device structure is the introduction of the InAsSbP barrier layer and window layer, which provides the advantage of suppressing the diffusion dark current and surface leakage current, respectively.

In the abovementioned epi-structure, there are three interfaces of InAsSbP barrier/InAs substrate, InAs absorber/InAsSbP barrier, and InAs absorber / InAsSbP window, which involve the lattice mismatch of InAsSbP and InAs.

The HRXRD patterns of the three device samples D1-D3 are shown in Fig. 4. We state below how to adjust the growth parameters to obtain the appropriate lattice mismatch. There are two most important growth parameters that affect the lattice mismatch, one is the growth temperature, and the other is the liquid composition of melt for the InAsSbP epilayer. The growth temperature and liquid composition of the three device samples are shown in Table 1. If InAsSbP peak in XRD is expected to shift towards higher angle (decrease the lattice mismatch), we usually tend to increase the growth temperature and increase the phosphorus mole fraction in liquid composition. If InAsSbP peak in XRD is expected to shift towards the lower angle (increase the lattice mismatch), we usually tend to increase the antimony mole fraction in liquid composition while the growth temperature remains unchanged. The most important concern that the lattice mismatch of some device samples is an appropriate value of about 0.2%, but the surface morphology of the device samples is dark and not shiny, which means material quality is poor. In this situation we usually increase the growth temperature and increase the arsenic mole fraction in liquid composition, then the surface morphology becomes shiny and the lattice mismatch remains the same.

2.3 Device performance analysis

Typical I-V curves obtained at room temperature for the device samples D1-D3 are shown in Fig. 5. Obviously, the dark current of D2 sample is the lowest among the three device samples. Sample D2 shows an ideal I-V characteristic curve, the reverse leakage current of samples D1 and D3 increases rapidly with the increase of voltage, indicating that the device forms an obvious leak-

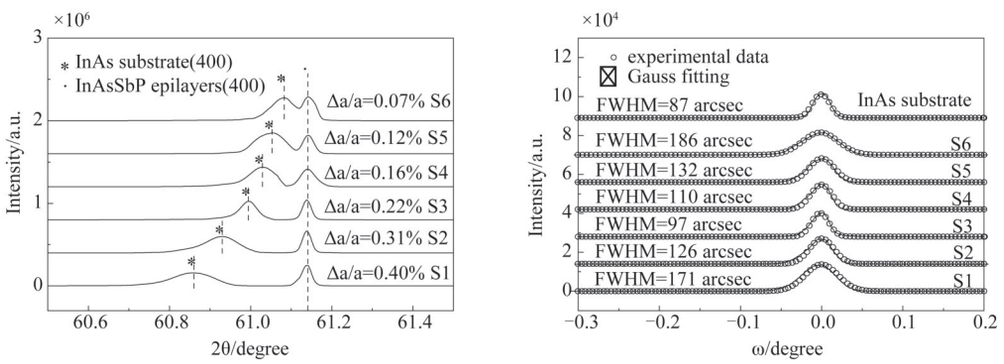

Fig. 1 (a) HRXRD patterns of samples S1-S6 and (b) rocking curves of (400) peaks of InAsSbP epilayer of samples S1-S6

图1 (a) S1-S6样品HRXRD图及(b) InAsSbP外延膜(400)摇摆曲线图

Table 1 Growth temperature T_g, liquid and solid composition of device samples with different lattice mismatches

表1 不同晶格失配的器件样品生长温度、液相组分、固相组分表

Sample	Lattice mismatch of InAsSbP/InAs	T_g/℃	Layer	Liquid composition (Mole fraction)				Solid composition ($InAs_{1-x-y}Sb_xP_y$)	
				X_L^{In}	X_L^{As}	X_L^{Sb}	X_L^{P}	x	y
D1	0.09	553	InAsSbP barrier	0.652 3	0.010 5	0.336 1	0.001 1	0.10	0.37
			InAs absorber	0.910 4	0.089 6	–	–	–	–
			InAsSbP window	0.652 3	0.010 5	0.336 1	0.001 1	0.10	0.37
D2	0.21	553	InAsSbP barrier	0.633 6	0.010 5	0.354 8	0.001 1	0.12	0.30
			InAs absorber	0.910 4	0.089 6	–	–	–	–
			InAsSbP window	0.633 6	0.010 5	0.354 8	0.001 1	0.12	0.30
D3	0.40	551	InAsSbP barrier	0.633 7	0.010 5	0.354 8	0.001 0	0.14	0.26
			InAs absorber	0.910 4	0.089 6	–	–	–	–
			InAsSbP window	0.633 7	0.010 5	0.354 8	0.001 0	0.14	0.26

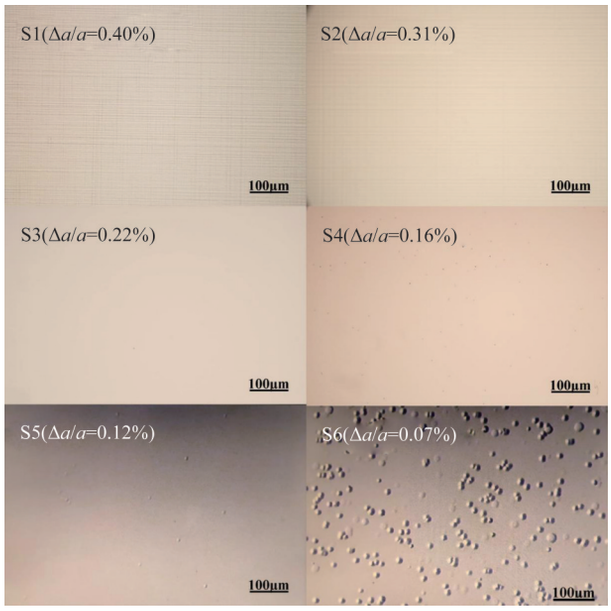

Fig. 2 Optical surface morphology of samples S1-S6
图2 S1-S6样品光学显微镜表面形貌图

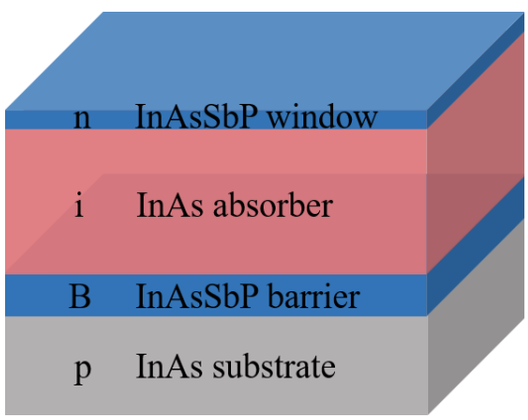

Fig. 3 The structure schematic of the device samples D1-D3
图3 D1-D3器件样品结构示意图

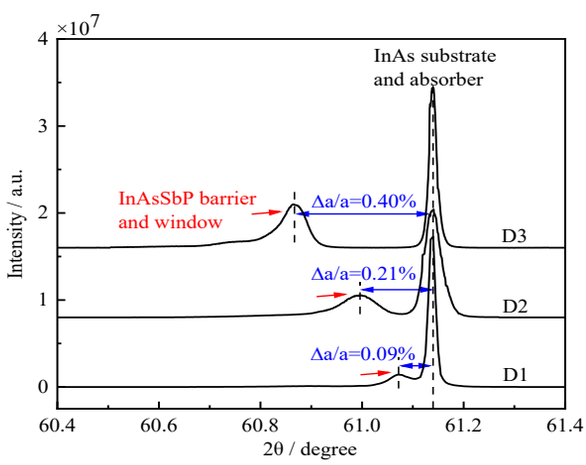

Fig. 4 The HRXRD patterns of the device samples D1-D3
图4 D1-D3器件样品XRD图

age channel.

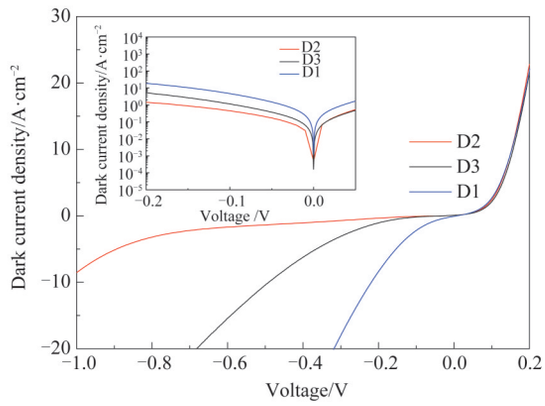

Fig. 5 *I-V* curves of device samples D1-D3
图5 D1-D3器件样品*I-V*曲线图

Figure 6 shows the room-temperature performance of the device sample D2. The peak responsivity is 0.62 A/W. The peak detectivities were calculated using the following equation[10].

$$D^* = \frac{R_i}{\sqrt{2qJ_d + \frac{4K_bT}{RA}}} \quad ,(1)$$

where R_i is the device responsivity, J_d is the dark current density, q is the electron charge, K_b is the Boltzamnn constant, T is the temperature, R is the dynamic resistance, and A is the detector area. The peak detectivity was calculated to be 6.8×10^9 cm $Hz^{1/2}W^{-1}$, which is nearly 1.5-2.5 times that of the Teledyne Judson Technologies [20] and the Hamamatsu Company[21]. Notably, among all the well-known commercial infrared detector suppliers, room-temperature InAs detectors are only provided by Teledyne Judson Technologies and Hamamatsu, which are global leaders for infrared detectors.

3 Conclusion

The paper reported the LPE growth of the high room-temperature performance mid-infrared InAs-based photodetector. It is proposed that careful control of the lattice mismatch between InAsSbP and InAs is crucial for obtaining the expected performances. In the InAs/InAsSbP system grown by Liquid Phase Epitaxy, it is found that the lattice mismatch between InAsSbP and InAs is not the smaller the better, but there is an appropriate value, which is about 0.20%. When the lattice mismatch deviates from this value, the surface morphology of the material deteriorates, this leads to the increase of the dark current of the detector. The detector architecture with the appropriate lattice mismatch was obtained by adjusting the growth parameters such as the mole fraction of the antimony, phosphorus and arsenic in liquid composition and the growth temperature. Finally, the infrared detector made from the device material with the appropriate lattice mismatch was fabricated, and its room-temperature detectivity is comparable to that of international com-

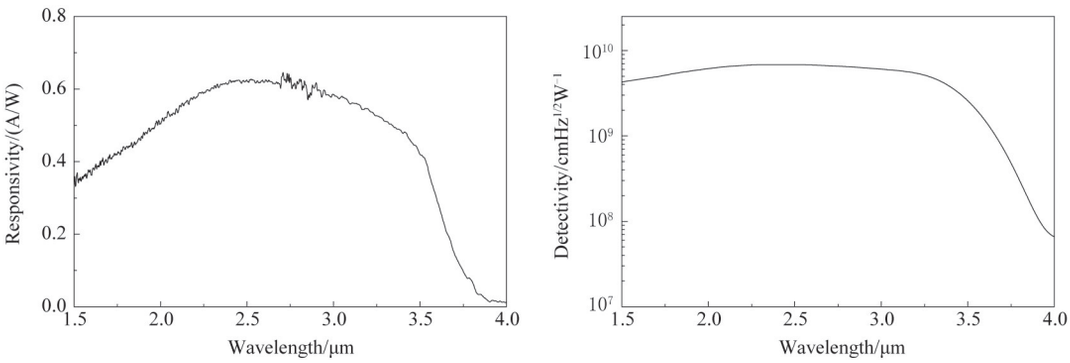

Fig. 6 The responsivity and detectivity of device sample D2 measured at room temperature
图6 D2器件样品室温光学响应率及探测率图

mercial InAs photodetectors.

References

[1] Flannigan L, Yoell L, Xu C Q. Mid-wave and long-wave infrared transmitters and detectors for optical satellite communications-a review[J]. *Journal of Optics*, 2022, **24**(4): 043002.

[2] Cao Y T, Wang G, Yan D G, *et al*. Two algorithms for the detection and tracking of moving vehicle targets in aerial infrared image sequences[J]. *Remote Sensing*, 2015, **8**(1): 28-28.

[3] Schubert M, Bttcher L, Gamper E, *et al*. Detectability of space debris objects in the infrared spectrum[J]. *Acta Astronautica*, 2022, **195**: 41-51.

[4] Zhu L, Deng Z, Huang J, *et al*. Low frequency noise-dark current correlations in HgCdTe infrared photodetectors[J]. *Optics Express*, 2020, **28**(16): 23660-23669.

[5] Bhan R K, Dhar V. Recent infrared detector technologies, applications, trends and development of HgCdTe based cooled infrared focal plane arrays and their characterization [J]. *Opto-Electronics Review*, 2019, **27**(2): 174-193.

[6] Maimon S, Wicks G W. nBn detector, an infrared detector with reduced dark current and higher operating temperature [J]. *Applied Physics Letters*, 2006, **89**(15): 4429.

[7] Du X, Savich G R, Marozas B T, *et al*. Suppression of lateral diffusion and surface leakage currents in nBn photodetectors using an inverted design[J]. *Journal of Electronic Materials*, 2018, **47**(2): 1038 - 1044.

[8] Du X, Marozas B T, Savich G R, *et al*. Defect-related surface currents in InAs-based nBn infrared detectors[J]. *Journal of Applied Physics*, 2018, **123**(21): 214504-1-214504-5.

[9] Deng G R, Yang W Y, Zhao P, *et al*. High operating temperature InAsSb-based mid-infrared focal plane array with a band-aligned compound barrier[J]. *Applied Physics Letters*, 2020, **116**(3): 031104.

[10] Deng G R, Yang W Y, Gong X X, *et al*. High-performance uncooled InAsSb-based pCBn mid-infrared photodetectors[J]. *Infrared Physics & Technology*, 2020, **105**: 103260.

[11] Tong J C, Tobing L, Qiu S P, *et al*. Room temperature plasmon-enhanced $InAs_{0.91}Sb_{0.09}$-based heterojunction n-i-p mid-wave infrared photodetector[J]. *Applied Physics Letters*, 2018, **113**(1): 011110.1-011110.5.

[12] Tong J C, Tobing L, Qian L, *et al*. $InAs_{0.9}Sb_{0.1}$-based hetero p-i-n structure grown on GaSb with high mid-infrared photodetection performance at room temperature[J]. *Applied Physics Letters*, 2018, **53**(18): 13010-13017.

[13] Suo F, Tong J C, Qian L, *et al*. Study of dark current in mid-infrared InAsSb-based hetero n-i-p photodiode[J]. *Journal of Physics D-Applied Physics*, 2018, **51**(27): 275102.

[14] Ting D Z, Soibel A, Khoshakhlagh A, *et al*. Mid-wavelength high operating temperature barrier infrared detector and focal plane array [J]. *Applied Physics Letters*, 2018, **113**(2): 021101.

[15] Soibel A, Ting D Z, Rafol S B, *et al*. Mid-wavelength infrared InAsSb/InAs nBn detectors and FPAs with very low dark current density [J]. *Applied Physics Letters*, 2019, **114**(16): 161103.

[16] Lin H Y, Zhou Z J, Xie H, *et al*. High-performance room-temperature extended-wavelength InAs-based middle-wavelength infrared photodetector[J].*Physica Status Solidi (A)- Applications and Materials Science*, 2021, **218**(18): 2100281.

[17] Krier A, Suleiman W, *et al*. Uncooled photodetectors for the 3 - 5 μm spectral range based on III - V heterojunctions[J]. *Applied Physics Letters*, 2006, **89**(8): 083512.

[18] Marcadet X, Rakovska A, Prevot I, *et al*. MBE growth of room-temperature InAsSb mid-infrared detectors [J]. *Journal of Crystal Growth*, 2001, **227**(1): 609-613.

[19] Saha S, Cassidy D T, Thompson D A. Investigation of cross-hatch in $In_{0.3}Ga_{0.7}As$ pseudo-substrates[J]. *Journal of Applied Physic*, 2013, **113**(12): 49-52.

[20] Teledyne Judson, *J12 series InAs detector*, (http://www.teledynejudson.com/products/indium-arsenide-detectors).

[21] Hamamatsu P.10090-01, *InAs Detector*, (https://www.hamamatsu.com/eu/en/product/type/P10090-01/index.html).